SIAM J. APPL. MATH.
Vol. 66, No. 6, pp. 1978–1997

CONVECTION EFFECTS IN THIN REACTION ZONES: APPLICATIONS TO BIACORE*

DAVID A. EDWARDS†

Abstract. Surface-volume reactions occur in many physical systems such as biological and industrial processes. Though traditionally modeled as a surface, the reaction zone is usually a thin layer (often a gel) abutting a flowing fluid or gas. Therefore, one would expect a more realistic model for the reacting zone to include the effects of transport in the gel. In this paper we examine the BIAcore, a device for measuring rate constants which has this geometry. To explain anomalous measurements from the device, it has been proposed that some flow penetrates into the dextran (gel) layer, thus enhancing transport. To analyze the reversible kinetics, asymptotic and singular perturbation techniques are used, yielding linear and nonlinear integrodifferential equations. Explicit and asymptotic solutions are constructed for cases motivated by experimental design. The results indicate that such flow penetration effects are bound to be negligible in surface-volume reactions, regardless of the flow model used.

Key words. asymptotic expansions, BIAcore, biochemical reactions, integrodifferential equations, reaction zone, singular perturbations

AMS subject classifications. 35B25, 35C20, 35K57, 45J05, 80A30, 92C45

DOI. 10.1137/040621831

1. Introduction.

In many physical systems, so-called "surface-volume" reactions occur. In the simplest model, one reactant (herein called the *receptor*) is confined to a two-dimensional surface, while the other (the *ligand*) floats free in (a possibly stirred) solution, and the reaction occurs only when the ligand interacts with the surface. However, since the receptors are three-dimensional molecules, they either form or are embedded in a thin *reaction zone* (such as a gel) near the surface. Given that many of these systems occur in the presence of an active flow, it is natural to inquire into the effects of the flow on the reaction zones.

Models of this type are applicable to various industries. The creation of alginate gel in the food industry is enhanced by the addition of a convective flow of reactant [27]. In bubble reactors, gas reacts with the liquid which impinges on the bubble surfaces [19]. Corrosive processes occur in such geometries [13]. Inorganic material synthesis can be enhanced if the templates are immersed in flow, rather than fixed-batch, reactors [20]. In high-pressure continuous-flow fixed-bed reactors, gels are introduced at the reaction surface to minimize hydrodynamics effects [14]. Harmful blood clots form when platelets adhere to foreign objects in the presence of blood flow [12]. Various biological processes ensue when ligands floating in the bloodstream bind to cell receptors which occupy a thin reaction zone about the cell membrane [11].

1.1. The BIAcore.

For the purposes of this paper, we focus on the BIAcore, which is a surface plasmon resonance (SPR) device for measuring rate constants. The configuration of the BIAcore is described in great detail elsewhere [16], [17], [18], [26]. For the purposes of this manuscript, we may consider the BIAcore to consist

*Received by the editors December 31, 2004; accepted for publication (in revised form) June 6, 2006; published electronically September 26, 2006. This work was supported by National Institute for General Medical Sciences grant 1R01GM067244-01.
http://www.siam.org/journals/siap/66-6/62183.html
†Department of Mathematical Sciences, University of Delaware, Newark, DE 19716-2553 (edwards@math.udel.edu).

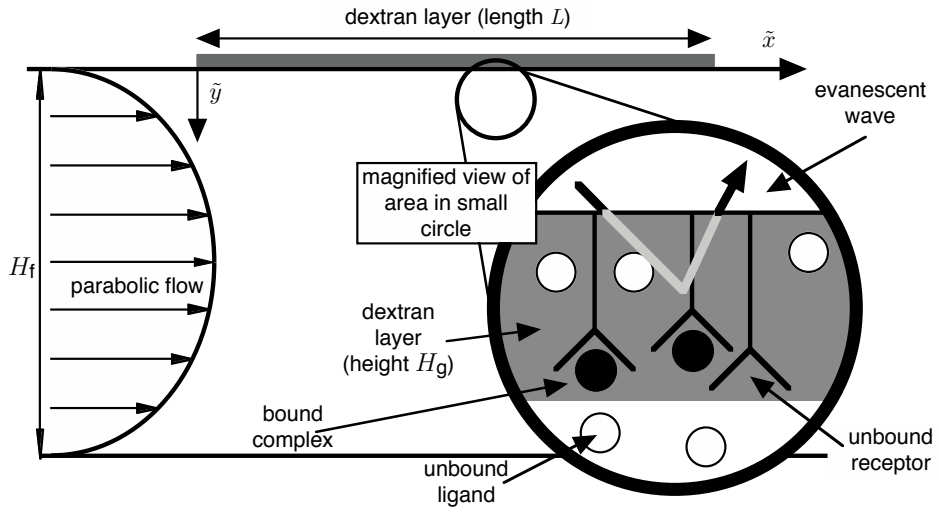

FIG. 1.1. *Schematic of BIAcore device. The coordinate system has its origin at the intersection of the $\tilde{y}$-axis and the dextran-flow interface.*

of a rectangular channel through which the ligand is convected in standard two-dimensional Poiseuille flow from $\tilde{x} = 0$, the inlet position (see Figure 1.1). Receptors are embedded in a thin dextran gel attached to the ceiling of the channel. Hence this device can serve as a representative of many physical systems of the type described above.

As the ligand diffuses to receptor sites, the binding process is measured by an evanescent wave that tracks mass changes in the dextran gel, as described more fully in section 6. This *sensogram* data is then transferred to a regression program which estimates the rate constants. During recent years, mathematical models of the BIAcore have become increasingly more sophisticated, treating many facets of its transport processes, including depletion of the free-flowing ligand along the channel [2], [3], [8], [21], [22]; diffusion in the gel [5], [25], [30], [31]; and signal decay associated with the measuring wave [6], [18], [25]. However, discrepancies still occur between measurements and simulations using the most sophisticated models [16], [24], [29].

To explain some anomalous observations, Witz [29] proposed that some of the buffer flow in the channel penetrates into the dextran gel, thus enhancing transport. In [7], Edwards formulated a mathematical model for this flow and analyzed it in the case where the reacting zone is treated as a surface. Now we shall treat the reaction zone as a layer.

As a first approximation, we model the dextran gel as a viscous fluid; others have treated it as a polymer brush [29]. We show that the physical parameter measuring penetration is $H_r = H_g/H_f$, the ratio of the heights of the gel and bulk flow regions. To leading order the flow adds a local depletion term to the mass action law for the bound state. When the Damköhler number Da is small, we obtain detailed expressions for the effect of penetration on the measurements. When $\mathrm{Da} = O(1)$ a nonlinear integral equation results, but the rate constants can easily be estimated using short-time asymptotics. We consider not only association, but also dissociation experiments. We also include the effect of evanescent wave decay in the measurement device.

All of our results indicate that flow penetration effects are very small. Such a conclusion arises from the geometry of the device, rather than from the model chosen for the dextran. Since the gel layer is so narrow compared to the rest of the device, velocities there will be small, no matter the actual transport model used. Clearly this result can be extended to the other physical systems described above.

2. Preliminaries. We consider the BIAcore to be divided into two regions, as shown in Figure 1.1: the open channel (the region $0 \le \tilde{y} \le H_{\rm f}$, where the subscript "f" stands for "flow") and the dextran gel layer (the region $-H_{\rm g} \le \tilde{y} \le 0$, where the subscript "g" stands for "gel"). We are interested in only that portion of the dextran layer which has length L, and so we take both regions to have $0 \le \tilde{x} \le L$.

2.1. Velocity profiles. The Reynolds number is small [7], so the flow in the channel is described by a simple one-dimensional laminar model. On the other hand, the dextran is a gel, and any true description of the flow therein would be quite complicated. For instance, Witz [29] considers the gel to be a polymer brush. For the purposes of this paper, we treat it merely as a very viscous fluid. This will necessarily misstate some quantitative features of the flow, but we shall show that such errors are negligible when analyzing sensogram data.

For simplicity, we introduce the following scalings for $\tilde{y}$ and the velocity field $\tilde{v}$:

$$y_{\rm f} = \frac{\tilde{y}}{H_{\rm f}}, \quad v_{\rm f}(y_{\rm f}) = \frac{\tilde{v}_{\rm f}(\tilde{y})}{V_{\rm f}}, \quad V_{\rm f} = \frac{\Delta p H_{\rm f}^2}{2\mu_{\rm f} L}, \quad y_{\rm g} = \frac{\tilde{y}}{H_{\rm g}}, \quad v_{\rm g}(y_{\rm g}) = \frac{\tilde{v}_{\rm g}(\tilde{y})}{V_{\rm g}}, \tag{2.1a}$$

$$V_{\rm g} = \frac{H_{\rm r}}{\mu_{\rm r}} V_{\rm f}, \quad H_{\rm r} = \frac{H_{\rm g}}{H_{\rm f}}, \quad \mu_{\rm r} = \frac{\mu_{\rm g}}{\mu_{\rm f}}, \tag{2.1b}$$

where μ is the bulk viscosity, V is the characteristic velocity in each region, and Δp is the (constant) pressure differential, which can be related to the known flow rate. Here (and throughout), if the same symbol appears both with and without tildes, the symbol with a tilde has dimensions, while the symbol without a tilde is dimensionless.

In (2.1b) the subscript "r" refers to "ratio," and we will use it in the same way (gel to flow) throughout. Using these scalings, it can be shown [7] that with suitable boundary and interface conditions, the velocity profiles are given by

$$v_{\rm f}(y_{\rm f}) = 1 - y_{\rm f}^2 + \frac{(y_{\rm f} - 1)(\mu_{\rm r} - H_{\rm r}^2)}{H_{\rm r} + \mu_{\rm r}}, \tag{2.2a}$$

$$v_{\rm g}(y_{\rm g}) = H_{\rm r}(1 - y_{\rm g}^2) + \frac{(y_{\rm g} + 1)(\mu_{\rm r} - H_{\rm r}^2)}{H_{\rm r} + \mu_{\rm r}}. \tag{2.2b}$$

Since solid dextran corresponds to $\mu_{\rm r} = \infty$, we might consider $\mu_{\rm r}$ as a large parameter to use in a perturbation approach. However, we can solve our problem for *any* $\mu_{\rm r}$ if we choose $H_{\rm r} \ll 1$, as motivated by its value in Table 4.1 below. Since $H_{\rm r}$ is simply a geometric parameter, such a choice will extend our results to other physical systems with thin reaction zones.

In the limit of small $H_{\rm r}$, (2.2b) becomes a nearly linear profile, corresponding to flow driven largely by shear from the bulk interface. Though using a more complicated polymer brush model for the gel leads to exponential and Bessel-function velocity profiles, these also reduce to linear profiles for small $H_{\rm r}$ [29]. Thus the two approaches are equivalent with a proper choice of $\mu_{\rm r}$.

2.2. Transport in the flow. In the flow, the ligand (concentration $\tilde{C}_{\rm f}$) travels both by convection and diffusion. However, the Peclét number in the flow, defined as

$$\text{Pe}_{\rm f} = \frac{H_{\rm f}^2/\tilde{D}_{\rm f}}{L/V_{\rm f}} = \frac{\text{characteristic diffusion time in flow}}{\text{characteristic convection time in flow}}, \tag{2.3}$$

is large (for a typical value, see Table 4.1 below). Here $\tilde{D}_{\rm f}$ is the molecular diffusion coefficient of the ligand in the flow. Hence one needs consider only the thin Lévêque boundary layer near $\tilde{y} = 0$ [3], which motivates the following scalings:

$$x = \frac{\tilde{x}}{L}, \quad y = \text{Pe}_{\rm f}^{1/3} y_{\rm f}, \quad t = \tilde{k}_{\rm on} C_{\rm u} \tilde{t}, \quad \tilde{C}_{\rm f}(\tilde{x}, \tilde{y}, \tilde{t}) = C_{\rm u}[1 - \text{Da} C_{\rm f}(x, y, t)], \tag{2.4}$$

where $\tilde{k}_{\rm on}$ is the association rate constant and $C_{\rm u}$ is the ligand concentration entering the device, which is used to create the dimensionless ligand concentration $C_{\rm f}$. Note that with our choice of scalings, the reaction time scale is the one of interest.

Here Da is the *Damköhler number*

$$\text{Da} = \frac{\tilde{k}_{\rm on}\tilde{R}_{\rm T}}{\tilde{D}_{\rm f}/(H_{\rm f}\text{Pe}_{\rm f}^{-1/3})} = \frac{\text{reaction ``velocity''}}{\text{diffusion ``velocity'' in boundary layer}}, \tag{2.5}$$

where $\tilde{R}_{\rm T}$ is the area density of receptor sites in the device. Da, which measures the effect of transport on the chemical reaction, characterizes the size of ligand depletion induced by the reaction, as shown in (2.4). Since $\text{Pe}_{\rm f} \propto V_{\rm f}$, $\text{Da} = 0$ corresponds to the case of infinitely fast flow where no depletion occurs. Most experiments are designed so that Da is small; hence the choice of scaling in (2.4) makes $C_{\rm f}$ a perturbation.

With these scalings, it can be shown [7] that the governing equations for $C_{\rm f}$ are

$$\frac{\partial^2 C_{\rm f}}{\partial y^2} = (v_0 + v_1 y)\frac{\partial C_{\rm f}}{\partial x}, \qquad C_{\rm f}(0, y, t) = 0, \quad C_{\rm f}(x, \infty, t) = 0, \tag{2.6a}$$

$$v_0 \equiv v_{\rm f}(0)\text{Pe}_{\rm f}^{1/3} = \frac{H_{\rm r}\text{Pe}_{\rm f}^{1/3}(H_{\rm r}+1)}{H_{\rm r}+\mu_{\rm r}}, \qquad v_1 \equiv v_{\rm f}'(0) = \frac{\mu_{\rm r} - H_{\rm r}^2}{H_{\rm r}+\mu_{\rm r}}. \tag{2.6b}$$

The scaling of v_0 in (2.6b) is chosen so that our results transition smoothly to the solid dextran case in the limit of large $\mu_{\rm r}$.

For the size of the transport processes to be comparable, the length scale in the Lévêque boundary layer in the fluid (where convection and diffusion balance) should be on the order of that in the gel. This implies that

$$H_{\rm g} = O(H_{\rm f}\text{Pe}_{\rm f}^{-1/3}) \Longrightarrow H_{\rm r} = O(\text{Pe}_{\rm f}^{-1/3}). \tag{2.7}$$

Such a scaling makes v_0 into an $O(1)$ quantity as long as we treat $\mu_{\rm r}$ as $O(1)$. Equation (2.7) also motivates the choice of $H_{\rm r}$ as a small parameter, since $\text{Pe}_{\rm f} \gg 1$. Unfortunately, (2.7) is rather a weak bound. From Table 4.1 below we have that $H_{\rm r} \ll \text{Pe}_{\rm f}^{-1/3}$, and so velocities in the gel will be comparatively small. Again, this result will hold for other systems with similar geometries.

To solve for $C_{\rm f}$, we use Laplace transforms (denoted with a hat) in the x-direction. To understand the gel dynamics, we need the value of $\hat{C}_{\rm f}$ only at the flow-gel interface $y = 0$. In particular, it can be shown [7] that $\hat{C}_{\rm f}$ satisfies

$$\hat{C}_{\rm f}(0, t) = \frac{\text{Ai}(s^{1/3}v_0/v_1^{2/3})}{(sv_1)^{1/3}\,\text{Ai}'(s^{1/3}v_0/v_1^{2/3})}\frac{\partial \hat{C}_{\rm f}}{\partial y}(0, t). \tag{2.8}$$

3. Dynamics in the dextran layer.

3.1. Transport. In the dextran gel, the reaction occurs only inside the pores, so it is the concentration of ligand *per fluid volume* that is important. To convert to this quantity, we simply divide $\tilde{C}_{\mathrm{g}}$, the concentration of ligand in the gel matrix, by the volume fraction ϕ of pores in the gel. (ϕ is also called the *partition coefficient*.) Motivated by this reasoning and (2.4), we choose the following scaling for $\tilde{C}_{\mathrm{g}}$:

$$\tilde{C}_{\mathrm{g}}(\tilde{x},\tilde{y},\tilde{t}) = \phi C_{\mathrm{u}}[1 - \mathrm{Da} C_{\mathrm{g}}(x, y_{\mathrm{g}}, t)]. \tag{3.1a}$$

Because the dextran layer is often treated as a surface, $\tilde{R}_{\mathrm{T}}$ is usually quoted as an *area* concentration. To convert this to a volume concentration, we simply divide by the width of the layer H_{g}, and hence we have an appropriate scaling for $\tilde{B}$:

$$B_{\mathrm{g}}(x, y_{\mathrm{g}}, t) = \frac{H_{\mathrm{g}}}{\tilde{R}_{\mathrm{T}}} \tilde{B}_{\mathrm{g}}(\tilde{x},\tilde{y},\tilde{t}). \tag{3.1b}$$

Though the receptor density may initially be nonuniform [15], [23], for now we take it to be uniform, since the error introduced from such an assumption is small [9].

In the dextran gel, the ligand travels both by convection and diffusion. Its evolution is also affected by binding. Since the concentration of available receptors is so much greater than the ligand concentration [5], the $\partial C_{\mathrm{g}}/\partial t$ term in the transport equation may be neglected. Moreover, $H_{\mathrm{g}} \ll L$, and so diffusion in the x-direction can be neglected.

Lastly, the Peclet number in the gel is given by

$$\mathrm{Pe}_{\mathrm{g}} = \frac{H_{\mathrm{g}}^2/\tilde{D}_{\mathrm{g}}}{L/V_{\mathrm{g}}} = \frac{H_{\mathrm{r}}^3}{\mu_{\mathrm{r}}} \frac{\tilde{D}_{\mathrm{f}}}{\tilde{D}_{\mathrm{g}}} \mathrm{Pe}_{\mathrm{f}} = \frac{1}{\mu_{\mathrm{r}}} \frac{\tilde{D}_{\mathrm{f}}}{\tilde{D}_{\mathrm{g}}} O(v_0^3), \tag{3.2}$$

where we have used (2.1) and (2.7). Here $\tilde{D}_{\mathrm{g}}$ is the diffusion constant in the dextran gel. The analysis in [7], which considers the case of a surface reaction, contains terms only up to $O(v_0)$. The same sort of analysis will hold here (as shown below), and thus we may ignore convection in the ligand transport equation. Physically, the small size of Pe_{g} in (3.2) shows that diffusion is the dominant transport process in the layer, not convection. Thus the dominant effect of flow penetration is a slip condition on the bulk flow.

Hence the leading-order dimensionless ligand transport equation is given by

$$\frac{\partial^2 C_{\mathrm{g}}}{\partial y_{\mathrm{g}}^2} = -D \frac{\partial B}{\partial t}, \tag{3.3a}$$

$$D = \frac{\tilde{D}_{\mathrm{f}}/(H_{\mathrm{f}} \mathrm{Pe}_{\mathrm{f}}^{-1/3})}{\phi \tilde{D}_{\mathrm{g}}/H_{\mathrm{g}}} = \frac{\text{diffusion velocity in diffusive boundary layer}}{\text{diffusion velocity in dextran}}. \tag{3.3b}$$

We solve (3.3a) by writing our solution as the sum of a particular solution A_{p} and a homogeneous solution A_{h}, as follows:

$$C_{\mathrm{g}}(x, y_{\mathrm{g}}, t) = -D A_{\mathrm{p}}(x, y_{\mathrm{g}}, t) + A_{\mathrm{h}}(x, y_{\mathrm{g}}, t), \tag{3.4}$$

where A_{p} satisfies

$$\frac{\partial^2 A_{\mathrm{p}}}{\partial y_{\mathrm{g}}^2} = \frac{\partial B}{\partial t}, \qquad \frac{\partial A_{\mathrm{p}}}{\partial y_{\mathrm{g}}}(x, -1, t) = 0, \qquad A_{\mathrm{p}}(x, 0, t) = 0. \tag{3.5}$$

The homogeneous problem is most easily solved in Laplace transform space. Solving the homogeneous form of the operator in (3.3a) subject to a no-flux condition at the channel wall $y = -1$, we determine that $\hat{A}_\mathrm{h}$ is a function of t only. At the flow-gel interface, the flux and ligand concentration per fluid volume must be continuous. Combining these conditions with (2.8) and using the transform of (3.4), we obtain

$$\hat{A}_\mathrm{h}(t) = -\frac{\mathrm{Ai}(s^{1/3}v_0/v_1^{2/3})}{(sv_1)^{1/3}\,\mathrm{Ai}'(s^{1/3}v_0/v_1^{2/3})}\frac{\partial \hat{A}_\mathrm{p}}{\partial y_\mathrm{g}}(0,t). \tag{3.6}$$

Since we cannot invert (3.6) in closed form, we use the fact that we consider the dextran to be a very viscous fluid, so $v_0 \to 0$. Formally, there are two ways to justify this from (2.6b). The first, physically intuitive, reasoning is to say that $\mu_\mathrm{r} \to \infty$. The second, more consistent from a mathematical point of view, is to take $H_\mathrm{r} \to 0$. Then expanding (3.6) to leading two orders in v_0 and inverting, we obtain the following:

$$A_\mathrm{h}(x,t) = \frac{1}{(3v_1)^{1/3}\Gamma(2/3)}\int_0^x \frac{\partial A_\mathrm{p}}{\partial y_\mathrm{g}}(x-\xi,0,t)\frac{d\xi}{\xi^{2/3}} - \frac{v_0}{v_1}\frac{\partial A_\mathrm{p}}{\partial y_\mathrm{g}}(x,0,t) + O(v_0^2). \tag{3.7}$$

Note from (3.5) that

$$\frac{\partial A_\mathrm{p}}{\partial y_\mathrm{g}}(x,0,t) = \int_{-1}^0 \frac{\partial B}{\partial t}\,dy_\mathrm{g};$$

in other words, the derivative is simply the average rate of binding in the layer at fixed x. Thus the integral term in (3.7) has an elegant physical interpretation, namely that the deficit in the ligand concentration at position x is the accumulation of the reaction that has occurred upstream. The effect of the slip velocity is to introduce the *local* reaction into the computation of the ligand deficit through the second term in (3.7).

When expanding (3.6) to obtain the expansion in (3.7), we tacitly assumed that $s^{1/3}v_0 \ll 1$. However, Laplace transform theory states that small x corresponds to large s, so this assumption does not hold in the limit of small x. Fortunately, the BIAcore returns measurements not of B, but of its average over the entire layer and some scanning range $x_\mathrm{min} \le x \le x_\mathrm{max}$:

$$\bar{B}(t) = \frac{1}{x_\mathrm{max} - x_\mathrm{min}}\int_{x_\mathrm{min}}^{x_\mathrm{max}}\int_{-1}^0 B(x,y_\mathrm{g},t)\,dy_\mathrm{g}\,dx, \tag{3.8}$$

where x_min is bounded away from zero. Since $x = 0$ is out of the scanning range, we may confidently use our results to analyze sensogram data.

3.2. Reaction. The bound state evolves according to a standard bimolecular mass action law. Using the scalings in (2.4) and (3.1) leads to the dimensionless form

$$\frac{\partial B}{\partial t} = (1-B)(1-\mathrm{Da}C_\mathrm{g}) - KB, \quad K = \frac{\tilde{k}_\mathrm{off}}{\tilde{k}_\mathrm{on}C_\mathrm{u}}, \tag{3.9a}$$

$$B(x,y_\mathrm{g},0) = B_\mathrm{i}, \tag{3.9b}$$

where $\tilde{k}_\mathrm{off}$ is the dissociation rate constant and K is the dimensionless affinity constant. Though the theory can handle general initial conditions for B, in practice the initial condition is always spatially uniform. For an association experiment, initially there is no bound state. For a dissociation experiment, we start with the steady state of (3.9a), which will be shown to be a constant.

Since A_{p} depends on $\partial B/\partial t$, substitution of (3.4) and (3.7) into (3.9a) would yield a nonlinear integrodifferential equation, and an exact solution would have to be obtained numerically. However, asymptotic results can be derived in physically relevant regimes.

4. Small Da results. Equation (3.9a) shows that $\mathrm{Da} = 0$ corresponds to the well-mixed case where there is no depletion. When designing experiments, scientists strive to keep Da as small as possible to minimize transport effects [28]. Therefore, we now specialize to the case of small Da by introducing the following expansion:

$$B(x, y_{\mathrm{g}}, t) = B_0(x, y_{\mathrm{g}}, t) + \mathrm{Da} B_1(x, y_{\mathrm{g}}, t) + o(\mathrm{Da}). \tag{4.1}$$

4.1. Association experiment. We begin by considering an association experiment as described in section 3. If we substitute (4.1) into (3.9), we find to leading order that the ligand concentration does not contribute. Hence we are in the well-mixed case, the solution of which is given by

$$B_0(x, y_{\mathrm{g}}, t) = \frac{1 - e^{-\alpha t}}{\alpha} + B_{\mathrm{i}} e^{-\alpha t} = \bar{B}_0(t), \tag{4.2}$$

which leads to the following expression for A_{p}:

$$A_{\mathrm{p}} = \frac{dB_0}{dt} \frac{y_{\mathrm{g}}(y_{\mathrm{g}} + 2)}{2}. \tag{4.3}$$

Since A_{p} is independent of x, it is simple to use (4.3) in (3.7) and compute that

$$A_{\mathrm{h}}(x, t) = \frac{dB_0}{dt} h(x), \qquad h(x) = \frac{3^{2/3} x^{1/3}}{v_1^{1/3} \Gamma(2/3)} - \frac{v_0}{v_1}. \tag{4.4}$$

The value of $A_{\mathrm{h}}(x, t)$ in (4.4) is exactly the value of $C_{\mathrm{f}}(x, 0, t)$ obtained if the reacting zone is treated as (instead of a layer) a two-dimensional surface at $x = 0$. In that case, $D = 0$, and hence there is no contribution from A_{p} in (3.4).

Substituting (4.3) and (4.4) into (3.4), we obtain

$$C_{\mathrm{g}}(x, y_{\mathrm{g}}, t) = \frac{dB_0}{dt} h_{\mathrm{g}}(x, y_{\mathrm{g}}), \qquad h_{\mathrm{g}}(x, y_{\mathrm{g}}) = \left[-D \frac{y_{\mathrm{g}}(y_{\mathrm{g}} + 2)}{2} + h(x) \right]. \tag{4.5}$$

Thus, as in [5], the effects of the variables x and y decouple. We also note that (4.3) is exactly the same as in [5], which considered the no-penetration case. Hence the effect of flow penetration appears only in the homogeneous part. Since the velocity in the layer is negligible at this order, the flow simply provides a slip condition for the bulk, which then couples to the receptor layer through the flow-gel interface conditions.

Substituting (4.2) and (4.5) into the next order of our expansion of (3.9) and solving, we have the following:

$$B_1 = \left[\frac{(e^{-\alpha t} - 1)\chi}{\alpha} - Kt \right] \frac{\chi e^{-\alpha t}}{\alpha} h_{\mathrm{g}}(x, y_{\mathrm{g}}). \tag{4.6}$$

Then averaging, we obtain

$$\bar{B}_1 = \frac{\chi e^{-\alpha t}}{\alpha} \left[\frac{(e^{-\alpha t} - 1)\chi}{\alpha} - Kt \right] \bar{h}_{\mathrm{g}}, \qquad \bar{h}_{\mathrm{g}} = \frac{D}{3} + \bar{h}. \tag{4.7}$$

TABLE 4.1
Parameter values for Figures 4.1 *and* 4.2.

Parameter	Value	Parameter	Value
B_{i}	0	Pe_{f}	3.72×10^{2}
C_{T} (mol/cm^3)	10^{-11}	t	$10^{-3}\,\tilde{t}$/s
D	1.20×10^{-1}	$x_{\max}$	7.92×10^{-1}
Da	10^{-1}	$x_{\min}$	2.08×10^{-1}
H_{r}	2×10^{-3}	α	2
K	1	χ	1
$\tilde{k}_{\mathrm{on}}$(cm^{3}mol^{-1}s^{-1})	10^{8}		

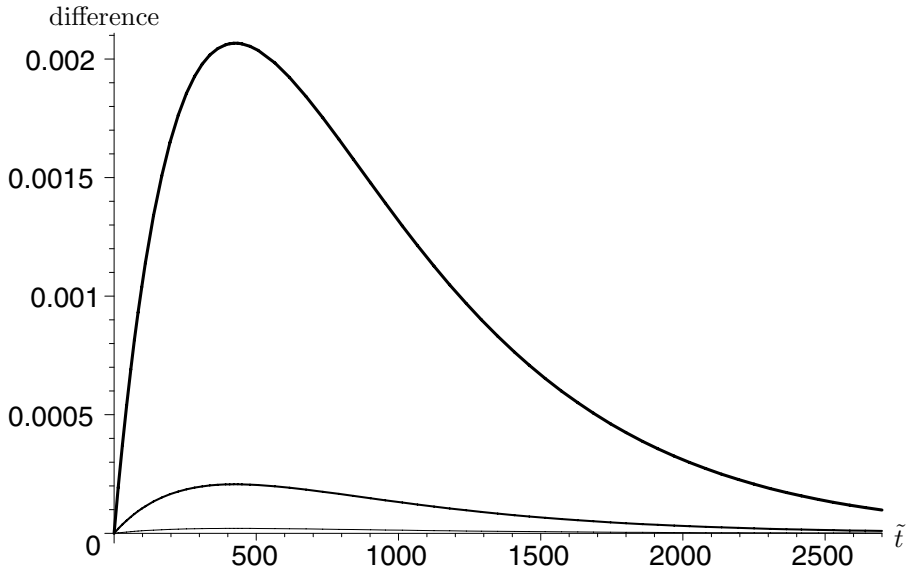

FIG. 4.1. *Absolute difference between* (4.7) *with* $\mu_{\mathrm{r}} = \infty$ (*solid dextran*) *and* μ_{r} *finite for* (*in decreasing order of thickness*) $\mu_{\mathrm{r}} = 1,\ 10,\ 100$. *Relative difference is about* 1%. *Association experiment.*

Aficionados of perturbation theory will note the term in (4.7) proportional to $te^{-\alpha t}$, similar to a secularity in a two-timing exercise. As $t \to \infty$, $B_0 = O(1)$ and $\mathrm{Da}B_1 \ll B_0$, so from an experimental standpoint, this is not a problem. However, it can be shown [3], [8] that a multiple-scale expansion is formally required. Though we could construct such an expansion for this case, it will not be illuminating.

We use the parameters listed in Table 4.1 to plot our solutions. The parameter values are from [7], with the exception of the value for D, which is from [6].

Figure 4.1 shows the effect of μ_{r} on $\bar{B}_1$ plotted against the *dimensional* time $\tilde{t}$ (in seconds) for various values of μ_{r}. We use the dimensional time in order to compare better with sensogram data. Note that in every case the difference is quite small due to the low value of H_{r}. In particular, even the error for $\mu_{\mathrm{r}} = 1$ (corresponding to the absence of a dextran layer) is only $O(H_{\mathrm{r}})$. In addition, the difference is positive; that is, allowing the flow to penetrate into the dextran layer enhances the association process. Since H_{r} is a geometrical parameter, this order estimate holds for other physical systems of this type.

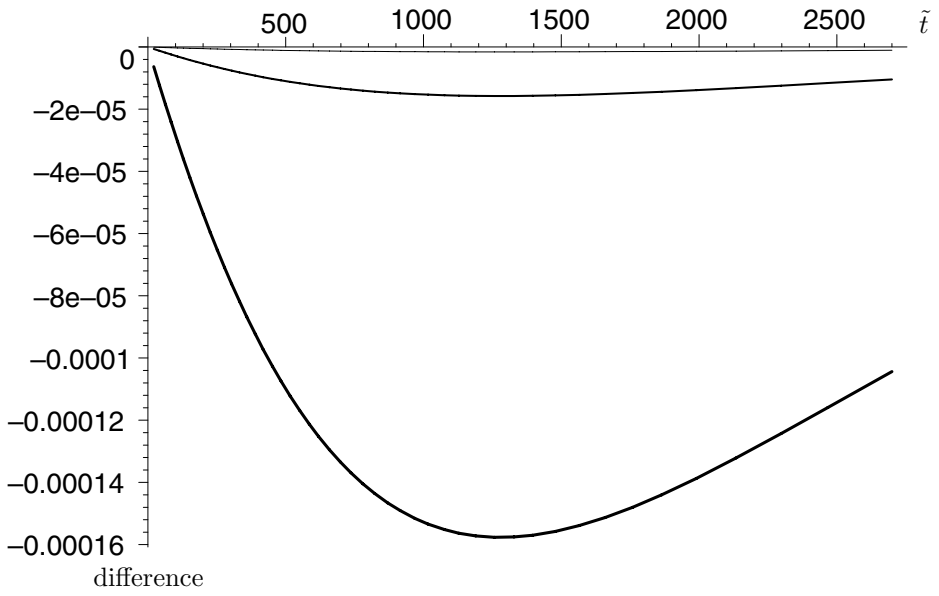

FIG. 4.2. *Absolute difference between effective rate constant solution* $\bar{B}$ *of* (4.8) *with* $\mu_r = \infty$ (*solid dextran*) *and* μ_r *finite for* (*in decreasing order of thickness*) $\mu_r = 1, 10, 100$. *Relative difference is about* 0.04%. *Association experiment.*

In Figure 4.1 (and throughout this manuscript) we graph the absolute difference because it is that difference which will be measured by the device and plotted on the sensogram. Obviously small differences will be masked by the underlying noise in any experiment. However, for comparison purposes and to extend our results to other physical systems, we also compute the relative difference. The case with $\mu_r = \infty$, graphed in Figure 1 of [5], shows that B_1 is on the order of 0.2, so the differences shown in Figure 4.1 are on the order of 1%. (Note this is the difference in $\bar{B}_1$, not in the whole solution, which would include the much greater contribution from $\bar{B}_0$.)

These results may be stated more simply in the context of an *effective rate constant* (ERC) equation, as outlined in [5], [8], and [21]. Substituting (4.5) into (3.9a), we have

$$\frac{\partial B}{\partial t} = (1 - B)\left[1 - \mathrm{Da}\frac{dB_0}{dt}h_g(x)\right] - KB + O(\mathrm{Da}^2),$$

which we may rearrange and average to obtain

$$\frac{d\bar{B}}{dt} = \frac{1 - \alpha\bar{B}}{1 + \mathrm{Da}(1 - \bar{B})\bar{h}_g} + O(\mathrm{Da}^2). \tag{4.8}$$

Equation (4.8) is an ODE for $\bar{B}$, the actual sensogram data produced by the BIAcore, and hence the solution requires no postprocessing averaging step. Equation (4.8) is in the form obtained previously [5], albeit with a different value of $\bar{h}$. This is consistent with [4], where it is shown that if B_0 is spatially uniform, the ERC approximation is robust to *any* geometry or flow.

Figure 4.2 shows the effect of μ_r on our ERC solution. The absolute error here is an order of magnitude smaller than that in Figure 4.1. This is because Figure 4.1

shows errors in $\bar{B}_1$, which have to be multiplied by Da (0.1 in our graphs) to obtain the error in the full solution as shown in Figure 4.2. The relative error here is around 0.1%, as can be seen by comparison with the full solution in Figure 1 of [8]. As before, flow penetration enhances the association process.

4.2. Dissociation experiment. A typical BIAcore experimental run begins with an association experiment run to completion. At this stage, pure buffer solution (inlet concentration zero) is injected into the device, initiating the dissociation process. This second experiment then provides additional data for rate constant estimation.

The initial condition for this phase of the experiment is the steady state of (3.9a). Since there is no flux of ligand through the exterior wall, one finds from (3.3a) that the steady state of C_{g} must be a constant. By using continuity arguments at the interface, one finds that this constant must be zero. Thus the steady state of (3.9a) is

$$B_{\mathrm{s}} = \alpha^{-1}, \tag{4.9}$$

where the subscript "s" refers to "steady state." Since (4.9) provides the initial condition for the dissociation problem, we are justified in always taking a constant initial condition for B.

With no ligand injected into the device, the equation analogous to (3.9a) becomes

$$\frac{\partial B}{\partial t} = (1-B)(-\mathrm{Da}C_{\mathrm{g}}) - KB. \tag{4.10}$$

Thus in this case $C_{\mathrm{g}} \leq 0$. The analysis proceeds in a manner analogous to the association experiment; the relevant results are given by

$$B_0(x,t) = \bar{B}_0(t) = \frac{e^{-Kt}}{\alpha}, \tag{4.11a}$$

$$\bar{B}_1 = \frac{K}{\alpha}\left(t + \frac{e^{-Kt}-1}{K\alpha}\right)\bar{h}_{\mathrm{g}}e^{-Kt}, \tag{4.11b}$$

where $\bar{h}_{\mathrm{g}}$ is given in (4.7). The same secularity problem appears with more obvious effects, since in the dissociation experiment the second term in the expansion can become larger than the first. Again, we restrict ourselves to the case where $\mathrm{Da}t = O(1)$, since constructing the multiple-scale expansion is not illuminating.

With the inlet value 1 absent from the concentration term in (4.10), the expression analogous to (4.8) is given by

$$\frac{d\bar{B}}{dt} = \frac{-K\bar{B}}{1+\mathrm{Da}(1-\bar{B})\bar{h}_{\mathrm{g}}} + O(\mathrm{Da}^2), \tag{4.12}$$

as in [5].

5. Moderate Da results. Since C_{g} depends on B, (3.9a) is nonlinear if $\mathrm{Da} = O(1)$. Thus to obtain analytic solutions we resort to short-time asymptotics by assuming a solution of the form

$$B(x,y_{\mathrm{g}},t) = B_{\mathrm{i}} + \beta(x,y_{\mathrm{g}})t + o(t), \qquad A_{\mathrm{p}}(x,y_{\mathrm{g}},t) = A_{\mathrm{p},1}(x,y_{\mathrm{g}}) + o(1), \tag{5.1a}$$

$$A_{\mathrm{h}}(x,t) = A_{\mathrm{h},1}(x) + o(1). \tag{5.1b}$$

5.1. Association experiment. Substituting (5.1) into (3.4), (3.9a), and (3.5), we have, to leading order in t,

$$C_{\mathrm{g}} = -DA_{\mathrm{p},1} + A_{\mathrm{h},1},$$

$$\beta = (1 - B_{\mathrm{i}})[1 - \mathrm{Da}(-DA_{\mathrm{p},1} + A_{\mathrm{h},1})] - KB_{\mathrm{i}}, \tag{5.2a}$$

$$\frac{\partial^2 A_{\mathrm{p},1}}{\partial y_{\mathrm{g}}^2} = \beta, \qquad \frac{\partial A_{\mathrm{p},1}}{\partial y_{\mathrm{g}}}(x,-1) = 0, \qquad A_{\mathrm{p},1}(x,0) = 0. \tag{5.2b}$$

Since (5.2a) is linear, it is most convenient to work in Laplace transform space. The relationship between $\hat{A}_{\mathrm{h},1}$ and $d\hat{A}_{\mathrm{p},1}/dy_{\mathrm{g}}(0)$ is exactly the same as in the transform of (3.7). Upon substituting that expression into the transform of (5.2) and solving, we obtain a form for $\hat{A}_{\mathrm{p},1}$ that depends explicitly on $d\hat{A}_{\mathrm{p},1}/dy_{\mathrm{g}}(0)$. Some algebraic manipulation eliminates the unknown from our solution, yielding

$$\hat{A}_{\mathrm{p},1} = -\frac{\chi}{\lambda_{\mathrm{a}}^2 r_{\mathrm{a}} s}\left[1 - \frac{\cosh\lambda_{\mathrm{a}}(y_{\mathrm{a}}+1)}{\cosh\lambda_{\mathrm{a}}}\right]\left(1 + \frac{\nu_{\mathrm{a}}^{1/3}}{s^{1/3}}\right)^{-1}, \tag{5.3}$$

$$r_{\mathrm{a}} = 1 - (1 - B_{\mathrm{i}})\mathrm{Da}\frac{v_0}{v_1}\frac{\tanh\lambda_{\mathrm{a}}}{\lambda_{\mathrm{a}}}, \qquad \lambda_{\mathrm{a}}^2 = D\mathrm{Da}(1 - B_{\mathrm{i}}), \tag{5.4a}$$

$$\nu_{\mathrm{a}} = \frac{1}{3v_1}\left\{\frac{\Gamma(2/3)}{\Gamma(1/3)}\left[\frac{1}{\mathrm{Da}(1-B_{\mathrm{i}})}\frac{\lambda_{\mathrm{a}}}{\tanh\lambda_{\mathrm{a}}} - \frac{v_0}{v_1}\right]\right\}^{-3}, \tag{5.4b}$$

where the subscript "a" denotes "association." We have written (5.4b) in a form where the correction due to v_0 can be easily seen. Recall that in deriving this form, we have already taken an asymptotic limit for small v_0. Thus, we should expect that (5.3) will hold only for those Da where the first bracketed term is much larger than the second.

To simplify the interpretation of the data, we write the average (3.8) in dimensional form with the aid of (2.4):

$$\bar{B}(\tilde{t}) \sim B_{\mathrm{i}} + S\tilde{t}, \quad \tilde{t} \to 0,$$

$$S = \frac{\tilde{k}_{\mathrm{on}} C_{\mathrm{u}}\{\mathcal{I}[\beta; x_{\max}] - \mathcal{I}[\beta; x_{\min}]\}}{x_{\max} - x_{\min}}, \tag{5.5a}$$

$$\mathcal{I}[\beta; x] \equiv \int_0^x \int_{-1}^0 \beta(\xi, y_{\mathrm{g}})\, dy_{\mathrm{g}}\, d\xi. \tag{5.5b}$$

Substituting (5.3) into the Laplace transform of (5.2b) and inverting, we have

$$\mathcal{I}[\beta; x] = \frac{\chi e^{-\nu_{\mathrm{a}} x}}{\nu_{\mathrm{a}} r_{\mathrm{a}}}\left[e^{\nu_{\mathrm{a}} x} - 1 - \left|P\left(\frac{4}{3}, -\nu_{\mathrm{a}} x\right)\right| + \left|P\left(\frac{5}{3}, -\nu_{\mathrm{a}} x\right)\right|\right]\frac{\tanh\lambda_{\mathrm{a}}}{\lambda_{\mathrm{a}}}, \tag{5.6a}$$

where P is the normalized *lower* incomplete gamma function whose definition is [1]

$$P\left(\frac{m}{3}, -\nu_{\mathrm{a}} x\right) = \frac{\gamma(m/3, -\nu_{\mathrm{a}} x)}{\Gamma(m/3)}. \tag{5.6b}$$

In the limit that $D \to 0$, $\lambda_{\mathrm{a}} \to 0$ and (5.6a) reduces to the result in the surface reaction case [7].

To estimate the rate constants from an experiment, we first run the association experiment to steady state. This will yield an estimate for α, and hence K, from (4.9). To calculate $\tilde{k}_{\mathrm{on}}$, we use the linear fit S from our short-time data in (5.5a) to

TABLE 5.1
Parameter values for Figures 5.1 *and* 5.2.

Parameter	Value	Parameter	Value
$\tilde{D}_{\mathrm{f}}$ (cm^2/s)	2.8×10^{-7}	L (cm)	2.4×10^{-1}
$\tilde{D}_{\mathrm{g}}$ (cm^2/s)	3.36×10^{-8}	R_{T} (mol/cm^2)	10^{-12}
$\tilde{k}_{\mathrm{off}}$ (s^{-1})	8.9×10^{-3}	ϕ	1

obtain $\tilde{k}_{\mathrm{on}}$. Since Da also depends on $\tilde{k}_{\mathrm{on}}$, the relationship between S and $\tilde{k}_{\mathrm{on}}$ is not a simple linear one. Using our estimates for K and $\tilde{k}_{\mathrm{on}}$ together, we may calculate $\tilde{k}_{\mathrm{off}}$.

We may asymptotically determine the behavior of S for small $\tilde{k}_{\mathrm{on}}$, which corresponds to small k. For small k, $r_{\mathrm{a}} \to 1$, $\lambda_{\mathrm{a}} \to 0$, and $\nu_{\mathrm{a}} \to 0$, so we have

$$S \sim \tilde{k}_{\mathrm{on}} C_{\mathrm{u}} \chi, \qquad \tilde{k}_{\mathrm{on}} \to 0. \tag{5.7}$$

Equation (5.7) merely shows that if there is no forward reaction ($\tilde{k}_{\mathrm{on}} = 0$), then there will be no change in the bound concentration from the initial state ($S = 0$).

At the other extreme, we cannot ascertain the behavior in the case that $k \to \infty$ due to the form of (5.4b). As k increases, so will Da, thus eventually causing the assumed ordering in (5.4b) to be violated. Essentially, because of the faster reaction, we cannot simply take the first-order convection correction; we must include additional terms in our analysis.

Since $\tanh \lambda_{\mathrm{a}} < 1$, we can still satisfy our ordering if we replace $\tanh \lambda_{\mathrm{a}}$ with 1 for simplicity. By doing so, we may construct a specific bound using the parameters in Table 5.1 (which come from [6] and [7]). The bound is calculated to be

$$k \ll 232 \mu_{\mathrm{r}}^2, \tag{5.8}$$

which is quadratic in μ_{r}—a much less restrictive bound than the linear bound in the surface reaction case [7].

5.2. Dissociation experiment. For the dissociation case, the initial condition is the steady state from the association problem, given in (4.9). In addition, the leading-order concentration is now 0, not 1. Essentially, only the parameters in the problem have changed, not the general structure. Therefore, the solution process follows as before, and our expression for $\mathcal{I}$ is

$$\mathcal{I}[\beta; x] = -\frac{K e^{-\nu_{\mathrm{d}} x}}{\alpha \nu_{\mathrm{d}} r_{\mathrm{d}}} \left[e^{\nu_{\mathrm{d}} x} - 1 - \left| P\left(\frac{4}{3}, -\nu_{\mathrm{d}} x\right) \right| + \left| P\left(\frac{5}{3}, -\nu_{\mathrm{d}} x\right) \right| \right] \frac{\tanh \lambda_{\mathrm{d}}}{\lambda_{\mathrm{d}}}, \tag{5.9}$$

$$\lambda_{\mathrm{d}}^2 = D \mathrm{Da} \left(\frac{K}{\alpha}\right), \qquad r_{\mathrm{d}} = 1 - \left(\frac{K}{\alpha}\right) \mathrm{Da} \frac{v_0}{v_1} \frac{\tanh \lambda_{\mathrm{d}}}{\lambda_{\mathrm{d}}}, \tag{5.10a}$$

$$\nu_{\mathrm{d}} = \frac{1}{3 v_1} \left\{ \frac{\Gamma(2/3)}{\Gamma(1/3)} \left[\frac{1}{\mathrm{Da}(K/\alpha)} \frac{\lambda_{\mathrm{d}}}{\tanh \lambda_{\mathrm{d}}} - \frac{v_0}{v_1} \right] \right\}^{-3}, \tag{5.10b}$$

where the subscript "d" refers to "dissociation." Similar to the previous subsection, in the limit that $D \to 0$, our results reduce to the surface reaction case in [7].

Using our new initial condition, we write our average as

$$\bar{B}(t) \sim \frac{1}{\alpha} + S\tilde{t}, \quad \tilde{t} \to 0,$$

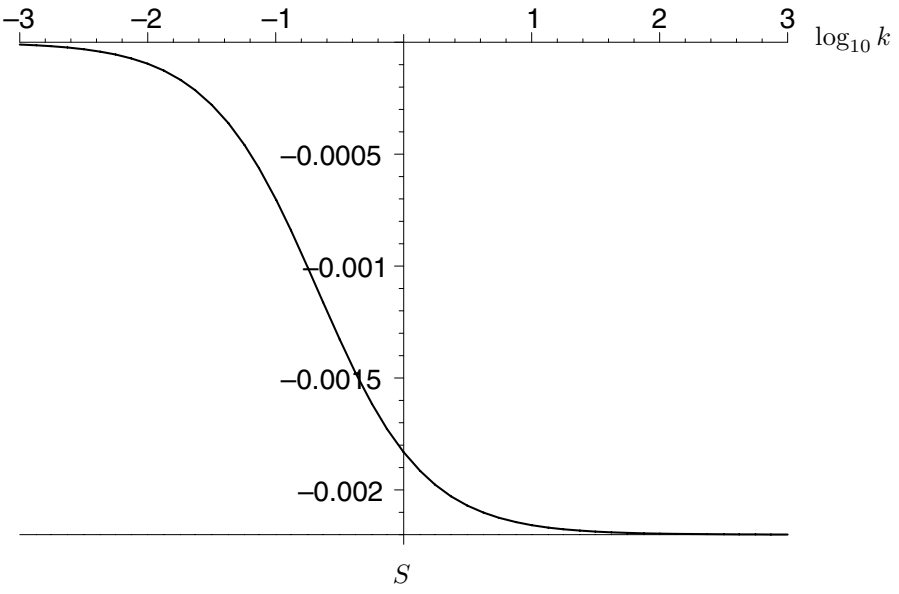

FIG. 5.1. *Thick line: S versus $\log_{10} k$, keeping $\tilde{k}_{\text{off}}$ fixed. Thin line: large-k asymptote. Dissociation experiment, $v_0 = 0$.*

where S is defined in (5.5a). Note from (5.9) that the slope is now negative, as expected for our dissociation problem.

We carefully analyze the behavior of S with respect to k, beginning with the case where $v_0 = 0$. In [5], the author kept K fixed and varied $\tilde{k}_{\text{on}}$, which necessitated (tacitly) varying $\tilde{k}_{\text{off}}$. In contrast, here we wish to keep $\tilde{k}_{\text{off}}$ fixed, which means that K will vary as $\tilde{k}_{\text{on}}$ does. This approach was taken in the study of flow penetration on the surface reaction case [7]. The value chosen for $\tilde{k}_{\text{off}}$ is listed in Table 5.1 and comes from [7].

In order to visualize the relationship between S and $\tilde{k}_{\text{on}}$, in Figure 5.1 we construct a curve using the parameters in Table 5.1 with $\mu_{\text{r}} = \infty$ (the solid dextran case). For convenience, we define the new variable

$$k = 10^{-9} \tilde{k}_{\text{on}} \frac{\text{mol} \cdot \text{s}}{\text{cm}^3}. \tag{5.11}$$

Since we take $B_{\text{i}} = 0$ for the association case, $\chi = 1$ and the solution is independent of K. It can be shown that the only qualitative difference between the graph here and with K fixed is in the asymptotes. (See [7] for a related discussion of the layer reaction case.)

For the small-$\tilde{k}_{\text{on}}$ asymptote, we first note from (5.10) that as $\tilde{k}_{\text{on}} \to 0$, $\lambda_{\text{d}} \to 0$, which causes the λ_{d} contribution to disappear, as in the previous subsection. In addition, $r_{\text{d}} \to 1$ and $\nu_{\text{d}} \to 0$. Thus we have that

$$S \sim -\tilde{k}_{\text{on}} C_{\text{u}}, \qquad \tilde{k}_{\text{on}} \to 0. \tag{5.12}$$

Note that (5.12) holds regardless of the value of v_0.

For the large-$\tilde{k}_{\text{on}}$ asymptote, we must restrict ourselves to the case with no flow:

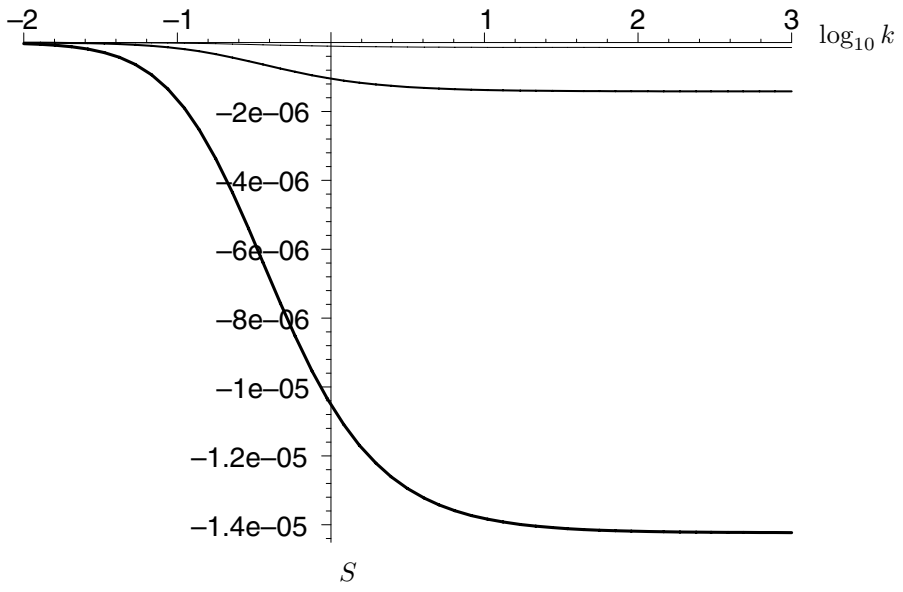

FIG. 5.2. *Absolute difference between S with $\mu_r = \infty$ (solid dextran) and μ_r finite versus $\log_{10} k$ for (in decreasing order of thickness) $\mu_r = 1$, 10, 100. Relative difference is about 1%. Dissociation experiment.*

$v_0 = 0$ and $v_1 = 1$, so $r_d = 1$. First, it is convenient to estimate λ_d in this limit:

$$\lim_{\tilde{k}_{on}\to\infty} \lambda_d \equiv \lambda_\infty = \left(\frac{\tilde{R}_T H_g}{\phi \tilde{D}_g} \frac{\tilde{k}_{off}}{C_u} \right)^{1/2}. \tag{5.13a}$$

In addition, we may use (5.10b) to calculate ν_∞ for this case:

$$\nu_\infty = \frac{1}{3\mathrm{Pe}_f} \left[\frac{\Gamma(1/3)}{\Gamma(2/3)} \frac{\tilde{R}_T H_f}{\tilde{D}_f} \frac{\tilde{k}_{off}}{C_u} \frac{\tanh \lambda_\infty}{\lambda_\infty} \right]^3, \quad v_0 = 0. \tag{5.13b}$$

Equations (5.13) illustrate a key difference between our analysis and that of [5]. In that work, K was kept fixed, so λ_d was unbounded as $\tilde{k}_{on} \to \infty$. This simplified $\mathcal{I}[\beta; x]$ greatly, leading to a relatively simple result. In our case, the asymptote has no convenient closed-form solution, but upon substituting (5.13) into (5.6a) and (5.5a), we obtain $S = -2.20 \times 10^{-3}$, which is exactly the asymptote in Figure 5.1.

Now that we have a baseline result for comparison, we next vary the viscosity ratio μ_r. Again we must preserve the assumed size ordering in (5.10b). Substituting our parameters into the above, we have

$$4.74 \times 10^{-1} \ll 16.2\mu_r, \tag{5.14}$$

which is simply a bound on μ_r that is always satisfied experimentally. Thus our expressions do not break down for large k as in the association case.

In Figure 5.2 we examine the effect of varying viscosity on the short-time asymptote S. As expected, the corrections are again small. The decrement to S increases

with decreasing μ_r, as lower μ_r means more convective transport, which enhances dissociation. By examining Figure 5.1, we see that the relative difference is about 1%.

6. Evanescent wave effects. The way in which an SPR device like the BIAcore measures binding is quite involved; here we present a brief summary. As binding occurs in the gel, the gel's index of refraction changes. A polarized light beam is aimed at the sensor surface at various angles. A sharp decrease in reflectivity is noted for a certain incidence angle, which can be related to the index of refraction and hence the binding. Since the strength of the evanescent wave (electric field) decays as it penetrates into the gel, the effect of binding on signal decays further from the surface $\tilde{y} = -H_g$ [10], [18].

By using a simple exponential decay model for the signal, we obtain the following result for the average $\bar{B}$, which replaces (3.8):

(6.1)
$$\bar{B}(t;\delta) = \frac{\delta}{(1-e^{-\delta})(x_{\max}-x_{\min})}\int_{x_{\min}}^{x_{\max}}\int_{-1}^{0} e^{-\delta(y_g+1)}B(x,y_g,t)\,dy_g\,dx, \qquad \delta = \frac{H_g}{H_w},$$

where H_w is the characteristic decay length of the wave. Here we include δ explicitly in the notation for $\bar{B}$ to indicate that we are including wave effects.

The only change to our work from previous sections is the calculation of averages. Since the leading-order solutions are independent of y_g, their averages do not change with the decaying signal strength.

6.1. Results for small Da. We begin by examining the small Da case. Using our averaging scheme in (6.1) to average h_g as given in (4.5) yields

$$\bar{h}_g(t;\delta) = D\frac{\delta^2 + 2[(\delta+1)e^{-\delta}-1]}{2\delta^2(1-e^{-\delta})} + \bar{h}. \tag{6.2}$$

It can be shown [6] that the term multiplying D is bounded between 1/3 (as in (4.7)) and 1/2; hence we expect the effect of the evanescent wave layer to be minimal. In order to plot some curves to verify this, we choose a typical decay length H_w from [25] and a typical gel width from [31]:

$$H_w = 9.5\times 10^{-6}\text{ cm}, \qquad H_g = 10^{-5}\text{ cm} \Longrightarrow \delta = 1.05. \tag{6.3}$$

As a naïve first approach, we might try to create a graph similar to Figure 4.1 to illustrate the changes of varying viscosity. However, we note from (4.4) and (6.2) that the only term involving μ_r is $\bar{h}$ (through the v_0 term). Hence the D term will always vanish when calculating

$$\bar{B}_1(\mu_r = \infty) - \bar{B}_1(\mu_r \neq \infty),$$

as in Figure 4.1. Since the D term includes the effect of decay, a graph of the above quantity will be the same whether or not decay is included.

The ERC solution does not have the unusual property described above, so to include the wave decay we substitute (6.2) into (4.8). In Figure 6.1 we plot the difference between the no-flow and viscous-flow cases of the ERC solution, including the wave decay. The graph is virtually indistinguishable from its analogue Figure 4.2, so the effect of decay is slight and the relative error is again around 0.04%.

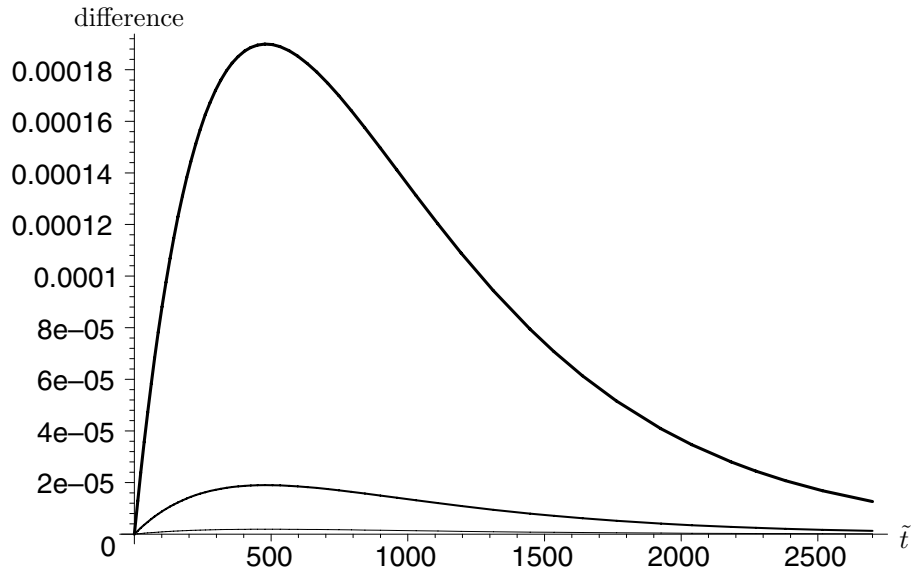

FIG. 6.1. *Difference between wave decay effective rate constant solution* $\bar{B}$ *of* (4.8) (*using* (6.1) *and* (6.2)) *with* $\mu_r = \infty$ (*solid dextran*) *and* μ_r *finite for* (*in decreasing order of thickness*) $\mu_r = 1$, 10, 100. *Relative difference is about* 0.04%. *Association experiment.*

For the dissociation experiment, the analysis is exactly analogous. The only difference is that rather than substituting (6.2) into (4.8), we substitute it into (4.12).

6.2. Results for moderate Da. The wave decay effect is more pronounced in the moderate Da case, in some cases leading to nonunique parameter estimates for the same data [6]. Proceeding in a manner analogous to (5.6a), we find that including the decay yields

$$\mathcal{I}[\beta;x] = \frac{\chi e^{-\nu_a x}}{2r_a\nu_a \cosh\lambda_a}\left[e^{\nu_a x} - 1 - \left|P\left(\frac{4}{3}, -\nu_a x\right)\right| + \left|P\left(\frac{5}{3}, -\nu_a x\right)\right|\right]$$
$$\times\left[\frac{e^{(\lambda_a-\delta)}-1}{\lambda_a-\delta} - \frac{e^{-(\lambda_a+\delta)}-1}{\lambda_a+\delta}\right]\frac{\delta}{1-e^{-\delta}}. \tag{6.4}$$

Note that the x-dependence is unchanged since the decay operates only in the y-direction.

Upon taking the limit for small $\tilde{k}_{on}$, the fact that $\lambda_a \to 0$ forces all the δ terms in the last line of (6.4) to cancel. Thus (5.7) still holds. This is because in this limit, the reaction is so slow that all transport effects are unimportant. Thus the binding will be uniform, and the wave decay cannot be discerned.

We demonstrate our results for varying μ_r in Figure 6.2. Since this is an association graph, the relevant restriction on k is given by (5.8), so the graphs end for different values of k. As before, the addition to S increases with decreasing μ_r, as lower μ_r means more convective transport, which enhances association. The actual value of S is essentially the negative of that shown in Figure 6.3, as can be seen from Figure 3 in [5]; hence the relative difference is about 1%.

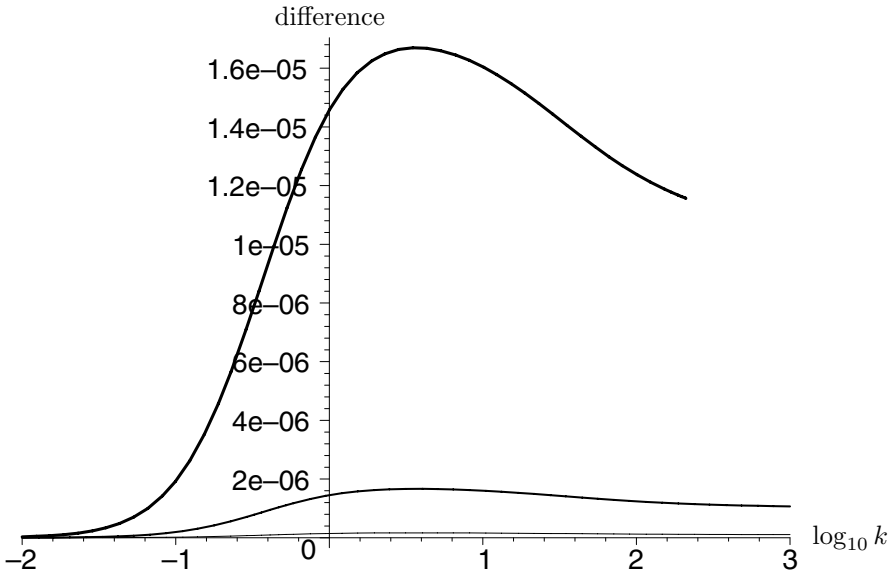

FIG. 6.2. *Absolute difference between S with $\mu_r = \infty$ (solid dextran) and μ_r finite versus $\log_{10} k$ for (in decreasing order of thickness) $\mu_r = 1$, 10, 100. Relative difference is about 1%. Association experiment, decay included.*

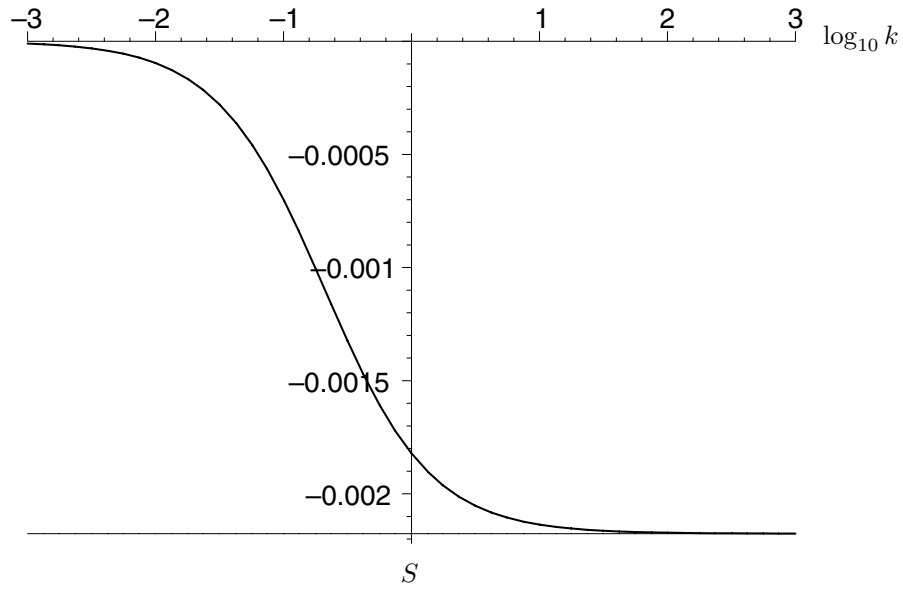

FIG. 6.3. *Thick line: S versus $\log_{10} k$, keeping $\tilde{k}_{\text{off}}$ fixed. Thin line: large-k asymptote. Dissociation experiment, $v_0 = 0$, wave decay considered.*

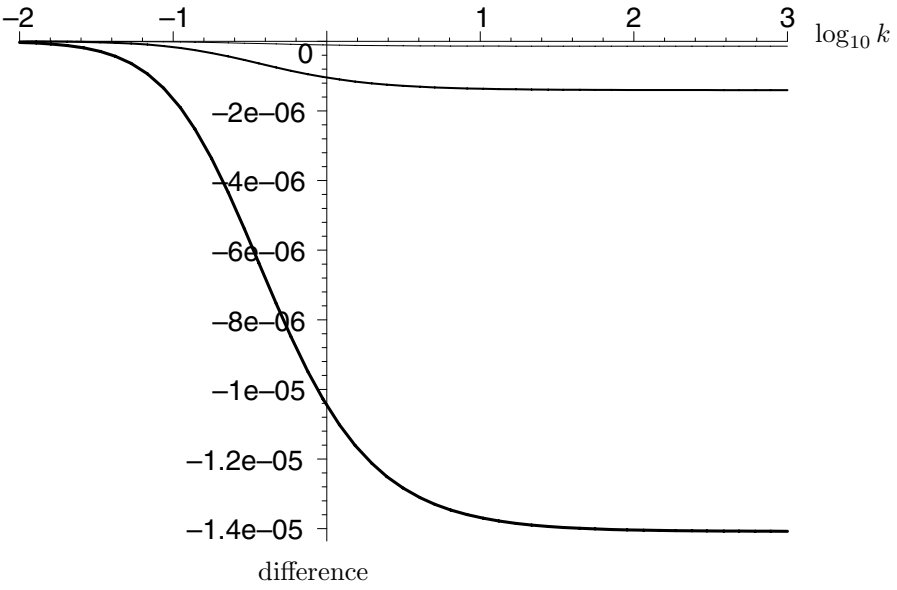

FIG. 6.4. *Absolute difference between S with $\mu_r = \infty$ (solid dextran) and μ_r finite versus $\log_{10} k$ for (in decreasing order of thickness) $\mu_r = 1$, 10, 100. Relative difference is about 1%. Dissociation experiment, decay included.*

For the dissociation case, the arguments are similar. The equation analogous to (5.9) is

$$\mathcal{I}[\beta; x] = -\frac{Ke^{-\nu_d x}}{2\alpha r_d \nu_d \cosh \lambda_d} \left[e^{\nu_d x} - 1 - \left| P\left(\frac{4}{3}, -\nu_d x\right)\right| + \left| P\left(\frac{5}{3}, -\nu_d x\right)\right|\right]$$

$$\times \left[\frac{e^{(\lambda_d - \delta)} - 1}{\lambda_d - \delta} - \frac{e^{-(\lambda_d + \delta)} - 1}{\lambda_d + \delta} \right] \frac{\delta}{1 - e^{-\delta}}. \tag{6.5}$$

As for the case without wave decay, earlier studies of the moderate Da case have kept K fixed and varied $\tilde{k}_{on}$ [6]. Thus, as in the previous subsection, in Figure 6.3 we present a demonstration graph to show what happens when we keep $\tilde{k}_{off}$ fixed instead. Again, the main difference lies in the asymptotes.

As above, when taking the limit for small $\tilde{k}_{on}$, the δ terms cancel. Thus the expression (5.12) for the small-$\tilde{k}_{on}$ asymptote still holds. For the large-$\tilde{k}_{on}$ asymptote in the no-flow case, we must use the expressions in (5.13). Substituting these parameters and our value of δ into (6.5) and (5.5a), we obtain $S = -2.18 \times 10^{-3}$, which is exactly the asymptote in Figure 6.3.

Lastly, we vary the viscosity ratio μ_r in Figure 6.4. Note that the corrections are again small and negative, as convection enhances dissociation. As in Figure 5.4, there are no restrictions on k because (5.14) is always satisfied. Therefore, our graphs go all the way to the right. Comparison with Figure 6.3 shows that the relative difference is again around 1%.

7. Conclusions. To explain BIAcore data that did not fit the traditional models, Witz [29] proposed that buffer flow from the channel penetrates into the dextran gel layer, enhancing transport. We have formulated a new model to include this effect. The key dimensionless parameter in this study is the small parameter H_r, which

measures the ratio of the widths of the gel and flow and hence characterizes the size of the velocity v_0 within the dextran gel. Its effect can be most readily seen in (3.7), where the slip condition at the flow-gel interface introduces a local depletion term that augments the integral depletion term from the no-flow case.

Since (3.9a) is a nonlinear equation, we obtained analytical results by introducing experimentally relevant simplifications. Most experiments are designed to have $\mathrm{Da} \ll 1$ to minimize transport effects, so we calculated the $O(\mathrm{Da})$ correction to the standard well-mixed case. The only effect of penetration is to introduce an additional term in $h(x)$, as defined in (4.4). We derived not only solution profiles for B, but also an ERC equation which can be used to fit sensogram data directly.

Some experiments cannot be designed such that $\mathrm{Da} \ll 1$, so we analyzed the moderate Da case by considering the short-time slope of the sensogram data. Corrections due to flow penetration appeared only in the parameter definitions in (5.4) and (5.10); the rest of the theory is the same as in the no-flow case [5]. The nature of our small-v_0 expansion dictated that we could not construct results for the case where $\mathrm{Da} \to \infty$; however, such conditions do not occur experimentally.

As in the small Da case, we examined both the association and dissociation phases of an experiment, providing (when possible) both the large- and small-$\tilde{k}_{\mathrm{on}}$ behavior of the short-time slope. In order to obtain results more consistent with experimental practice, we kept $\tilde{k}_{\mathrm{off}}$ fixed, in contrast to [5]. However, any differences between the papers were minor. In addition, since the inherent decay in the evanescent measuring wave affects only the averaging, not the transport, it was a simple matter to recast our previous results in this context.

In this manuscript we studied convection by modeling the dextran gel as a viscous fluid, though others have used more realistic polymer brush models [29]. Despite the simplicity of our model, the small thickness of the gel layer indicates that more realistic models will not produce qualitative changes in our results. We thus conclude that flow penetration effects are not likely to explain anomalous BIAcore measurements, and other effects, such as steric hindrance effects or conformational changes, should be investigated instead.

Moreover, since the size of the penetration effects are dictated by geometry, rather than properties of the gel, flow, or reactants, these insights can be extended to many similar physical systems. In particular, one may use gels and other compounds in reacting zones to reduce the size of hydrodynamic convective effects (as in [14]).

Acknowledgments. Portions of this manuscript were prepared during sabbatical stays at the Mathematical Biosciences Institute at The Ohio State University and the University of Maryland, Baltimore County.

REFERENCES

[1] M. Abramowitz and I. A. Stegun, eds., *Handbook of Mathematical Functions*, Appl. Math. Ser. 155, U. S. Department of Commerce, Washington, DC, 1972.

[2] S. J. Davis, E. A. Davies, A. N. Barclay, S. Daenke, D. L. Bodian, E. Y. Jones, D. I. Stuart, T. D. Butters, R. A. Dwek, and P. A. Van der Merwe, *Ligand binding by the immunoglobulin superfamily recognition molecule CD2 is glycosylation-independent*, J. Biol. Chem., 270 (1995), pp. 369–375.

[3] D. A. Edwards, *Estimating rate constants in a convection-diffusion system with a boundary reaction*, IMA J. Appl. Math., 63 (1999), pp. 89–112.

[4] D. A. Edwards, *Biochemical reactions on helical structures*, SIAM J. Appl. Math., 60 (2000), pp. 1425–1446.

[5] D. A. Edwards, *The effect of a receptor layer on the measurement of rate constants*, Bull. Math. Biol., 63 (2001), pp. 301–327.

[6] D. A. Edwards, *Refining the measurement of rate constants in the BIAcore*, J. Math. Biol., 49 (2004), pp. 272–292.
[7] D. A. Edwards, *Convection effects in the BIAcore dextran layer: surface reaction model*, Bull. Math. Biol., 68 (2006), pp. 627–634.
[8] D. A. Edwards, B. Goldstein, and D. S. Cohen, *Transport effects on surface-volume biological reactions*, J. Math. Biol., 39 (1999), pp. 533–561.
[9] D. A. Edwards and S. Swaminathan, *The effect of receptor site nonuniformity on the measurement of rate constants*, Appl. Math. Lett., 18 (2005), pp. 1101–1107.
[10] P. B. Garland, *Optical evanescent wave methods for the study of biomolecular reactions*, Quart. Rev. Biophys., 29 (1996), pp. 91–117.
[11] B. Goldstein and M. Dembo, *Approximating the effects of diffusion on reversible reactions at the cell surface: Ligand-receptor kinetics*, Biophys. J., 68 (1995), pp. 1222–1230.
[12] E. F. Grabowski, L. I. Friedman, and E. F. Leonard, *Effects of shear rate on the diffusion and adhesion of blood platelets to a foreign surface*, Ind. Eng. Chem. Fund., 11 (1972), pp. 224–232.
[13] X. Y. He, N. Li, and B. Goldstein, *Lattice Boltzmann simulation of diffusion-convection systems with surface chemical reaction*, Molec. Sim., 25 (2000), pp. 145–156.
[14] J. Jansen and B. Niemeyer, *Automated high-pressure plant for a continuous flow through a fixed bed investigation of hydrodynamic behaviour*, J. Supercrit. Fluids, 33 (2005), pp. 283–291.
[15] L. Joss, T. A. Morton, M. L. Doyle, and D. G. Myszka, *Interpreting kinetic rate constants from optical biosensor data recorded on a decaying surface*, Anal. Biochem., 261 (1998), pp. 203–210.
[16] R. Karlsson and A. Fält, *Experimental design for kinetic analysis of protein-protein interactions with surface plasmon resonance biosensors*, J. Immun. Methods, 200 (1997), pp. 121–133.
[17] R. Karlsson, A. Michaelson, and L. Mattson, *Kinetic analysis of monoclonal antibody-antigen interactions with a new biosensor based analytical system*, J. Immun. Methods, 145 (1991), pp. 229–240.
[18] B. Liedberg, I. Lundstrom, and E. Stenberg, *Principles of biosensing with an extended coupling matrix and surface-plasmon resonance*, Sens. Actuators B, 11 (1993), pp. 63–72.
[19] W. M. Long and L. V. Kalachev, *Asymptotic analysis of dissolution of a spherical bubble (case of fast reaction outside the bubble)*, Rocky Mountain J. Math., 30 (2000), pp. 293–313.
[20] S. Mann, S. L. Burkett, S. A. Davis, C. E. Fowler, N. H. Mendelson, S. D. Sims, D. Walsh, and N. T. Whilton, *Sol-gel synthesis of organized matter*, Chem. Mater., 9 (1997), pp. 2300–2310.
[21] T. Mason, A. R. Pineda, C. Wofsy, and B. Goldstein, *Effective rate models for the analysis of transport-dependent biosensor data*, Math. Biosci., 159 (1999), pp. 123–144.
[22] D. G. Myszka, X. He, M. Dembo, T. A. Morton, and B. Goldstein, *Extending the range of rate constants available from BIAcore: Interpreting mass transport influenced binding data*, Biophys. J., 75 (1998), pp. 583–594.
[23] D. J. O'Shannessy, M. Brigham-Burke, and K. Peck, *Immobilization chemistries suitable for use in the BIAcore surface plasmon resonance detector*, Anal. Biochem., 205 (1992), pp. 132–136.
[24] S. Qian, *private communication*, University of Pennsylvania, Philadelphia, PA, 2004.
[25] P. Schuck, *Kinetics of ligand binding to receptor immobilized in a polymer matrix, as detected with an evanescent wave biosensor.* I. *A computer simulation of the influence of mass transport*, Biophys. J., 70 (1996), pp. 1230–1249.
[26] A. Szabo, L. Stolz, and R. Granzow, *Surface plasmon resonance and its use in bio-molecular interaction analysis (BIA)*, Curr. Opin. Struct. Biol., 5 (1995), pp. 699–705.
[27] H. Treml, S. Woelki, and H.-H. Kohler, *Theory of capillary formation in alginate gels*, Chem. Phys., 3 (2003), pp. 341–353.
[28] L. D. Ward and D. J. Winzor, *Relative merits of optical biosensors based on flow-cell and cuvette designs*, Anal. Biochem., 285 (2000), pp. 179–193.
[29] J. Witz, *Kinetic analysis of analyte binding by optical biosensors: Hydrodynamic penetration of the analyte flow into the polymer matrix reduces the influence of mass transport*, Anal. Biochem., 270 (1999), pp. 201–206.
[30] C. Wofsy and B. Goldstein, *Effective rate models for receptors distributed in a layer above a surface: Application to cells and BIAcore*, Biophys. J., 82 (2002), pp. 1743–1755.
[31] M. L. Yarmush, D. B. Patankar, and D. M. Yarmush, *An analysis of transport resistance in the operation of BIAcore™; Implications for kinetic studies of biospecific interactions*, Molec. Immunol., 33 (1996), pp. 1203–1214.